Journal of Alloys and Compounds 517 (2012) 9–13

Contents lists available at SciVerse ScienceDirect

Journal of Alloys and Compounds

journal homepage: www.elsevier.com/locate/jallcom

Near white light emission of BaY_2ZnO_5 doped with Dy^{3+} ions

Chih-Hao Liang[a], Lay-Gaik Teoh[b], Kuan Ting Liu[c], Yee-Shin Chang[d,*]

[a] Nano Materials Center, ITRI South, Industrial Technology Research Institute, Tainan 701, Taiwan
[b] Department of Mechanical Engineering, National Pingtung University of Science and Technology, Neipu, Pingtung 912, Taiwan
[c] Department of Electronic Engineering, Cheng Shiu University, Kaohsiung 347, Taiwan
[d] Department of Electronic Engineering, National Formosa University, Huwei, Yunlin 632, Taiwan

ARTICLE INFO

Article history:
Received 7 September 2011
Received in revised form
13 November 2011
Accepted 16 November 2011
Available online 28 November 2011

Keywords:
Oxides
Phosphor
Near-white-light emission

ABSTRACT

Controlling activator concentrations to possess near white light emission of BaY_2ZnO_5 doped with Dy^{3+} ions was performed using high energy vibrating milled solid-state reaction. The XRD patterns show that all of the peaks can be attributed to the BaY_2ZnO_5 orthorhombic structure, because that the BaY_2ZnO_5 and $BaDy_2ZnO_5$ are isostructures with a space group of *Pbnm*. Under ultraviolet (355 nm) excitation, a weak group of emission peaks appear for the $^4M_{21/2}{}^4I_{13/2} + {}^4K_{17/2} + {}^4F_{7/2} \rightarrow {}^6H_{13/2}$ transition at 453 nm, and two groups of strong emission peaks appear at 489 nm and 579 nm, corresponding to the $^4F_{9/2} \rightarrow {}^6H_{15/2}$ and $^4F_{9/2} \rightarrow {}^6H_{13/2}$ transitions of Dy^{3+} ions, respectively. The decay curve results indicate that the decay mechanism of the $^4F_{9/2} \rightarrow {}^6H_{13/2}$ transition is a single decay component between Dy^{3+} ions only. In addition, the asymmetry ratio, which is independent of Dy^{3+} ion concentration, remains at about 1.04, indicating that the symmetry of Dy^{3+} ions does not change with concentration. Concentration quenching occurs with x values above 0.07, and the critical distance is about 11.93 Å. The CIE color coordinates of $x = 0.320$ and $y = 0.389$ are located in the near white light region.

1. Introduction

In recent years, inorganic phosphors have been extensively investigated for application in various types of flat panel display (FPD), such as plasma display panels (PDPs), thin film electroluminescence devices (TFEL), field-emission displays (FEDs), and vacuum fluorescent displays (VFDs) [1–7]. Nichia Chemical and Osram control many of the patents on phosphors, leading outside manufacturers to invest in three-wavelength mixed white lights and the development of novel phosphors. Oxide phosphors have recently received a lot of attention for applications such as screens in PDPs and FEDs and for white-light-emitting diodes due to their higher chemical stability and resistance to moisture compared to those of sulfide/phosphors [8–10].

Rare earth ion-doped crystal has attracted considerable research interest due to their excellent luminescence properties [11]. The use of rare-earth element-based phosphors, based on line-type f–f transitions, can narrow emissions to the visible range, resulting in high efficiency and high lumen equivalence. Rare-earth Dy^{3+} ions have two dominant emission bands, one in the blue region (470–500 nm) and one in the yellow region (560–600 nm). The two emissions originate from $^4F_{9/2} \rightarrow {}^6H_{13/2}$ and $^4F_{9/2} \rightarrow {}^6H_{15/2}$ transitions of Dy^{3+} ions, respectively. The yellow emission of Dy^{3+} is especially hypersensitive ($\Delta L = 2$, $\Delta J = 2$) to the local environment, whereas the blue emission is not. Therefore, by suitably adjusting the yellow-to-blue intensity ratio, it is possible to obtain a phosphor with near-white-light emission. It is the candidate for the potential white light emission phosphor with a single emitting center for luminescent materials doped with Dy^{3+} ions [12,13].

BaY_2ZnO_5 is a kind of luminescence host with a stable crystal structure and high thermal stability. BaY_2ZnO_5 has an orthorhombic structure with a space group of *Pbnm* [7]. The basic structure of BaY_2ZnO_5 consists of YO_7, BaO_{11}, and ZnO_5 polyhedra. *Y* is 7-fold coordinated inside a monocapped trigonal prism. These prisms share edges to form wave-like chains parallel to the long *b*-axis, and two such units join to form the basic structure motif of Y_2O_{11}. It is well known that a given optical center in different host lattices exhibits different optical properties due to the changes of the surroundings of the center of a Dy^{3+}-doped phosphor. In the present study, BaY_2ZnO_5 phosphors doped with various Dy^{3+} ion concentrations were synthesized using a vibrating mill solid-state reaction and calcined at 1250 °C for 12 h in air. The structure and photoluminescence properties of BaY_2ZnO_5:Dy^{3+} were investigated.

2. Experimental procedure

2.1. Powder preparation

The Dy^{3+}-doped BaY_2ZnO_5 phosphors formulated $Ba(Y_{1-x}Dy_x)_2ZnO_5$, with x equal to 0.01. 0.2 were synthesized by a vibrating mill solid-state reaction using

* Corresponding author. Tel.: +886 5 6315684; fax: +886 5 6315643.
E-mail address: yeeshin@nfu.edu.tw (Y.-S. Chang).

0925-8388/$ – see front matter © 2011 Elsevier B.V. All rights reserved.
doi:10.1016/j.jallcom.2011.11.088

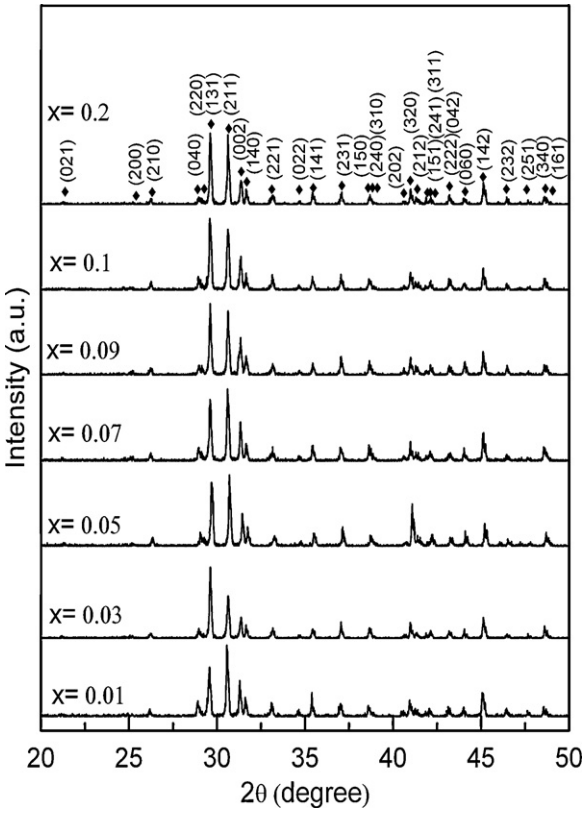

Fig. 1. X-ray diffraction patterns of BaY_2ZnO_5 doped with various Dy^{3+} concentrations and calcined at 1250 °C for 12 h.

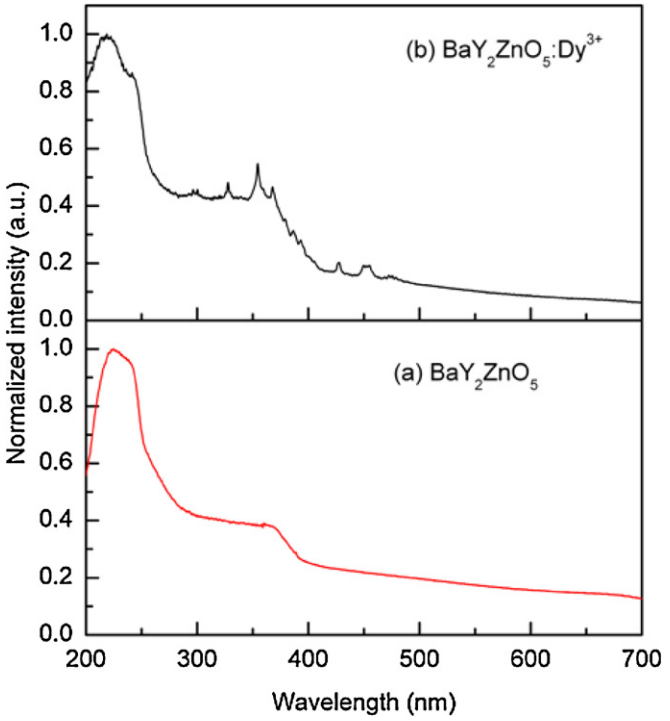

Fig. 2. Absorption spectra of (a) BaY_2ZnO_5 powders and (b) BaY_2ZnO_5:Dy^{3+} powders synthesized by a solid-state reaction and calcined at 1250 °C for 12 h.

barium carbide ($BaCO_3$), zinc oxide (ZnO), yttrium oxide (Y_2O_3), and dysprosium oxide (Dy_2O_3) with purities of 99.99% (purchased from Aldrich Chemical Company Inc.). The starting materials were weighed in a stoichiometric ratio and ground in a mechanically activated high-energy vibro-mill for 15 min with zirconia balls in a polyethylene jar. After mechanical mixing, the mixtures were calcined at 1250 °C in air for 12 h in a programmable furnace.

2.2. Characterization

The effects of Dy^{3+} doping and thermal treatment on the structure of the phosphors were studied by X-ray powder diffractometry (XRD, Rigaku Dmax-33) using Cu-Kα radiation with a source power of 30 kV and a current of 20 mA to identify the possible phases formed after heat treatment. Optical absorption spectra were measured in the range of 200–700 nm at room temperature using an ultraviolet–visible (UV–Vis) spectrophotometer (Hitachi U-3010). Both the excitation and luminescence spectra of the phosphors were recorded in the range of 200–700 nm on a fluorescence spectrophotometer (Hitachi F-4500) using a 150 W xenon arc lamp as the excitation source at room temperature.

3. Results and discussion

3.1. Structure

Fig. 1 shows the XRD patterns of BaY_2ZnO_5 doped with various Dy^{3+} ion concentrations and calcined at 1250 °C in air for 10 h. All samples exhibit a single phase which was identified as the BaY_2ZnO_5 phase (JCPDS Card No. 89-5856) without any impurities, indicating that the Dy^{3+} ions substituted the Y^{3+} ions. Using the Rietveld refinement method, Kaduk et al. [14] found that BaY_2ZnO_5 and $BaDy_2ZnO_5$ are isostructures with a space group of *Pbnm*. The full width at half maximum (FWHM) of the peaks did not show any obvious differences with an increase in Dy^{3+} concentration when trivalent terbium ions (0.97 Å) [15] were introduced to substitute the trivalent yttrium ions (0.96 Å) [15] in the $Ba(Y,Dy)_2ZnO_5$ system. The difference between Dy^{3+} and Y^{3+} ion radii is very small, and there are no charge compensation issues when Dy^{3+} ions substitute Y^{3+} ions in the $Ba(Y,Dy)_2ZnO_5$ lattice.

3.2. Absorption and excitation spectra

Fig. 2 shows the absorption spectra of the BaY_2ZnO_5 host and BaY_2ZnO_5:Dy phosphor. The host lattice shows two broad absorption maxima in the UV region. The strong absorption in the region from 200 to 270 nm is attributed to the band-to-band transitions, whereas the weaker broad peak from 270 to 400 nm can be attributed to the tightly bound Frankel excitons, which are usually observed close to the bandgap in large-bandgap crystals [16,17]. The absorption edge of the BaY_2ZnO_5 host is located at ~378 nm. For BaY_2ZnO_5:Dy^{3+}, there is a series of sharp absorption bands between 300 and 500 nm, which can be attributed to the typical f–f transitions of Dy^{3+} ions. The compounds exhibit an absorption peak between 220 and 300 nm due to the charge transfer state (CTS) of the Dy^{3+} and O^{2-} ions [13,18]. Fig. 3 shows the absorption and excitation spectra of the BaY_2ZnO_5:Dy^{3+} phosphor. The excitation spectra were monitored at an emission wavelength of 579 nm for the $^4F_{9/2} \rightarrow {}^6H_{13/2}$ transition. As can be seen, there is a series of sharp excitation peaks between 200 and 500 nm. The peaks can be divided into (1) a broad band centered at 243 nm, which contains CTS bands due to the dysprosium–oxygen interactions [13,18], and (2) a series of sharp peaks in the range of 220–500 nm, which are associated with the typical intra-4f transitions of the Dy^{3+} ions that appear at 300, 328, 339, 355, 368, 394, 428, 455, and 475 nm for each excitation peak (labeled 2–10) in the excitation spectrum, respectively, which are attributed to ($^6H_{15/2} \rightarrow {}^4K_{13/2} + {}^4H_{13/2}$), ($^6H_{15/2} \rightarrow {}^4K_{15/2}$), ($^6H_{15/2} \rightarrow {}^4I_{9/2} + {}^4G_{9/2}$), ($^6H_{15/2} \rightarrow {}^4M_{15/2} + {}^6P_{7/2}$), ($^6H_{15/2} \rightarrow {}^4I_{11/2}$), ($^6H_{15/2} \rightarrow {}^4M_{21/2}{}^4I_{13/2} + {}^4K_{17/2} + {}^4F_{7/2}$), ($^6H_{15/2} \rightarrow {}^4G_{11/2}$), and ($^6H_{15/2} \rightarrow {}^4I_{15/2}$), ($^6H_{15/2} \rightarrow {}^4F_{9/2}$) transitions [19,20]. The strongest peak is located at 355 nm, which can be assigned to the $^6H_{15/2} \rightarrow {}^4M_{15/2} + {}^6P_{7/2}$ transition, which is good agreement with the results of the absorption analysis.

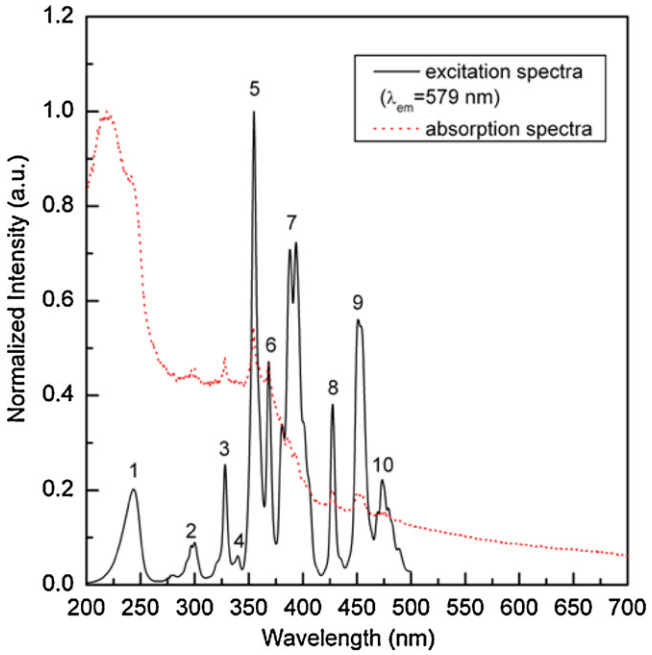

Fig. 3. Absorption spectra and PL excitation spectra of BaY_2ZnO_5:Dy^{3+} powders calcined at 1250 °C for 12 h. The excitation peaks labeled 1–10 are assigned to transitions between the ground $^6H_{15/2}$ level and the excited (1) charge transfer state band, (2) $^4K_{13/2}+{}^4H_{13/2}$, (3) $^4K_{15/2}$, (4) $^4I_{9/2}+{}^4G_{9/2}$, (5) $^4M_{15/2}+{}^6P_{7/2}$, (6) $^4I_{11/2}$, (7) $^4M_{21/2}+{}^4I_{13/2}+{}^4K_{17/2}+{}^4F_{7/2}$, (8) $^4G_{11/2}$, (9) $^4I_{15/2}$, and (10) $^4F_{9/2}$ levels, respectively.

3.3. Emission spectrum

In order to observe the emission behavior of BaY_2ZnO_5:Dy^{3+} phosphors, a 355-nm excitation wavelength was chosen because it is the strongest absorption peak for excitation. Fig. 4 shows the emission spectrum (λ_{ex} = 355 nm) of BaY_2ZnO_5 doped with Dy^{3+} ions and calcined at 1250 °C for 12 h in air. In the BaY_2ZnO_5:Dy^{3+} system, the concentration of Dy^{3+} ions did not affect the shape of the curves, but did affect the intensities of the emission spectra. In Fig. 4, the emission spectrum exhibits a weak group of emission peaks at 453 nm, corresponding to the $^4M_{21/2}{}^4I_{13/2}+{}^4K_{17/2}+{}^4F_{7/2}\rightarrow{}^6H_{13/2}$ transition, and two groups of strong peaks at 489 nm and 579 nm due to the $^4F_{9/2}\rightarrow{}^6H_{15/2}$ and $^4F_{9/2}\rightarrow{}^6H_{13/2}$ transitions of the Dy^{3+} ions, respectively.

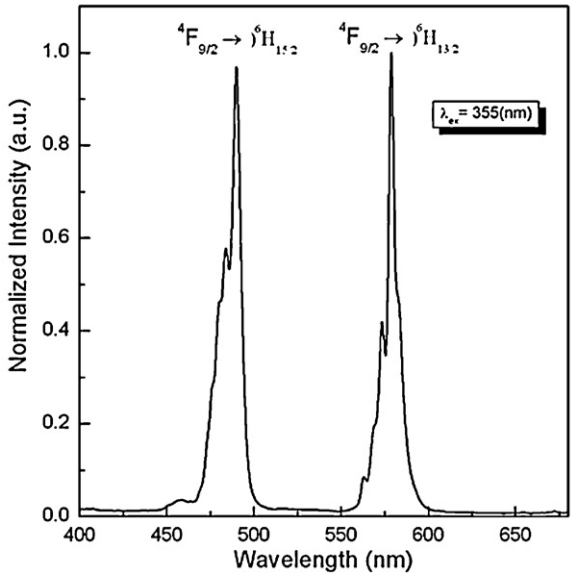

Fig. 4. Photoluminescence emission spectra of BaY_2ZnO_5:Dy^{3+} under an excitation wavelength of 355 nm.

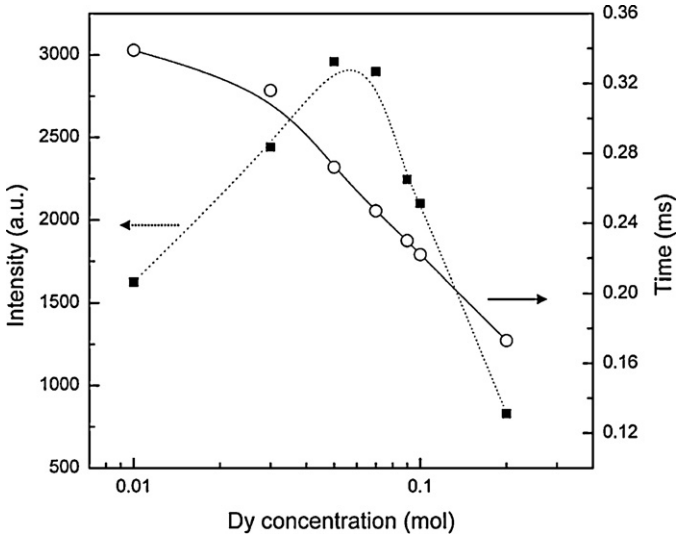

Fig. 5. Relationship of emission intensity and decay time of the $^4F_{9/2}\rightarrow{}^6H_{13/2}$ transition on Dy^{3+} concentration in BaY_2ZnO_5 under an excitation wavelength of 355 nm.

The $^4F_{9/2}\rightarrow{}^6H_{15/2}$ transition is the magnetic dipole transition, which hardly varies with the crystal field strength around the dysprosium ion. These groups of peaks for the $^4F_{9/2}\rightarrow{}^6H_{13/2}$ hypersensitive transition ($\Delta J=2$) of Dy^{3+} ions belongs to the forced electric dipole transition, which is strongly influenced by the outside environment for a low-symmetry lattice with no inversion center [12,19]. When the Dy^{3+} ions are located at low-symmetry local sites with no inversion center, the $^4F_{9/2}\rightarrow{}^6H_{13/2}$ emission transition is often prominent in the emission spectra [15]. From the results in Fig. 4, the intensity of the $^4F_{9/2}\rightarrow{}^6H_{13/2}$ transition is slightly higher than that of the $^4F_{9/2}\rightarrow{}^6H_{15/2}$ transition, which indicates that the Dy^{3+} ions are located at low-symmetry local sites with no inversion center in the BaY_2ZnO_5:Dy^{3+} phosphors. According to studies on the effect of the crystal field on the hypersensitive transition [21,22], the hypersensitive transition can be observed for a crystal structure with a point group of C_s, C_{1-6}, C_{2v}, C_{3v}, C_{4v}, and C_{6v}. BaY_2ZnO_5 has an orthorhombic structure with a space group of *Pbnm*. Y^{3+} ions occupy two 7-fold oxygen-coordinated sites with the same site symmetry as that of C_s. Therefore, the emission peak is dominated by the $^4F_{9/2}\rightarrow{}^6H_{13/2}$ transition of BaY_2ZnO_5:Dy^{3+} phosphors.

The emission ratio of the $^4F_{9/2}\rightarrow{}^6H_{13/2}$ transition and $^4F_{9/2}\rightarrow{}^6H_{15/2}$ transition (i.e., the asymmetry ratio) can be used as an index to measure the degree of distortion from the inversion symmetry of the local environment of Dy^{3+} ions in the host [22]. The asymmetry ratio on Dy^{3+} ion concentration in BaY_2ZnO_5:Dy^{3+} under an excitation of 355 nm is about 1.04. The ratio is independent of Dy^{3+} ion concentration, which indicates that the symmetry of Dy^{3+} ions does not change with concentration.

Fig. 5 shows the relationship between the intensity of the emission peak ($^4F_{9/2}\rightarrow{}^6H_{13/2}$) and the concentration of Dy^{3+} ions. It can be observed that the emission intensity increases with increasing Dy^{3+} ion concentration until it reaches a maximum value at 0.07 mol, and then decreases with further increases in the Dy^{3+} ion concentration. This behavior is due to the concentration quenching effect found in rare-earth-doped systems due to Dy^{3+}, Dy^{3+} mutual interactions [12,13,18].

In many cases, concentration quenching is due to energy transfer from one activator to another until the energy sink in the lattice

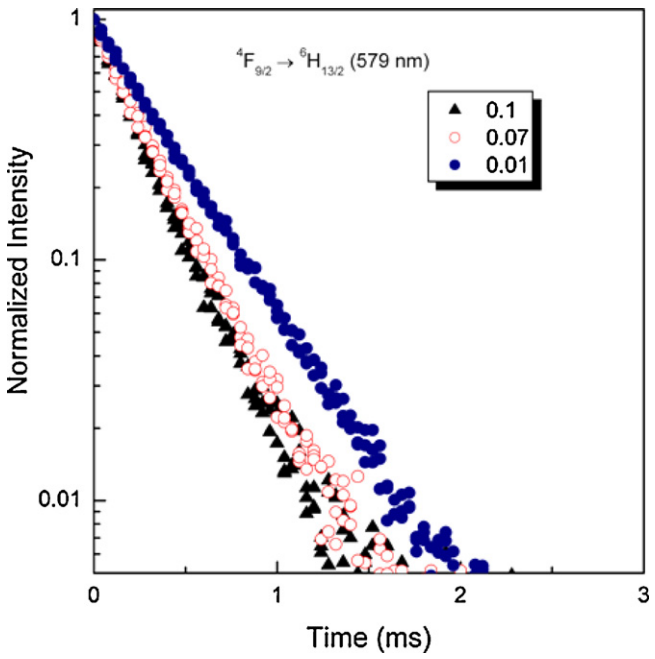

Fig. 6. Normalized decay curve of $^4F_{9/2} \rightarrow {}^6H_{13/2}$ emission for BaY_2ZnO_5 with various Dy^{3+} concentrations under an excitation wavelength of 355 nm.

is reached. Blasse [23] suggested that the critical distance (R_c) of energy transfer can be expressed by:

$$R_c = 2\left(\frac{3V}{4\pi x_c N}\right)^{1/3} \quad (1)$$

where x_c is the critical concentration, N is the number of Y^{3+} ions in the BaY_2ZnO_5 unit cell ($N = 8$ in BaY_2ZnO_5), and V is the volume of the unit cell ($V = 497.964 \times 10^{-30}\ m^3$ in this case) [14]. For the $^4F_{9/2} \rightarrow {}^6H_{13/2}$ transition, the critical concentration is estimated to be about $x_c = 0.07$, at which point the measured emission intensity and decay time begin to decrease rapidly. Using Eq. (1), R_c was calculated to be about 11.93 Å.

The effect of Dy^{3+} content on the $^4F_{9/2} \rightarrow {}^6H_{15/2}$ transition decay curves is shown in Fig. 6. The decay curves show a single exponential decay and do not obviously vary with Dy^{3+} ion concentration. The time-resolved $^4F_{9/2} \rightarrow {}^6H_{15/2}$ transition shows a single exponential decay even when all sites are occupied by Dy^{3+} ions. The decay curves can be represented by the equation:

$$I = I_0 \exp\left(\frac{-t}{\tau}\right) \quad (2)$$

where I and I_0 are the luminescence intensities at times t and 0, respectively, and τ is the radiative decay time. All the curves can be well fitted by a mono-exponential decay, revealing that the presence of the Dy^{3+} environment is unique.

Fig. 7 shows the CIE chromaticity diagram for BaY_2ZnO_5:Dy^{3+} phosphors. In BaY_2ZnO_5:Dy^{3+}, the concentration of Dy^{3+} ions did not affect the shape of emission curves and the asymmetry ratio. Therefore, the color coordinates of the emission is in the near-white-light region, with CIE color coordinates of $x = 0.320$ and $y = 0.389$, which is superior (white light color purity) to the other Dy^{3+}-doped phosphor such as YVO_4:$0.02Dy^{3+}$ ($x = 0.39$, $y = 0.46$) [12].

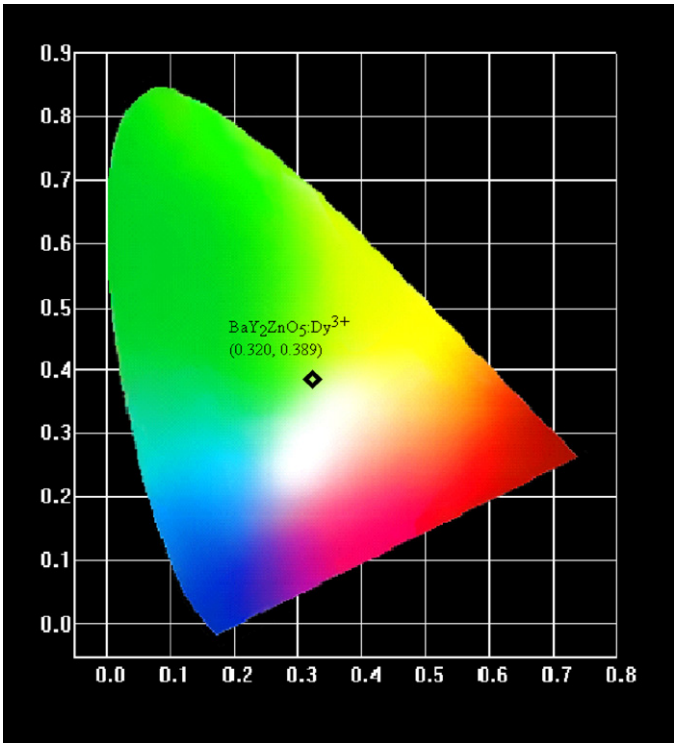

Fig. 7. CIE color coordinate diagram of BaY_2ZnO_5:Dy^{3+} phosphors.

4. Conclusion

A near-white-light emission phosphor, Dy^{3+}-doped BaY_2ZnO_5, was synthesized by a vibrating mill solid-state reaction, and its luminescence properties were investigated. The XRD patterns show that all of the peaks can be attributed to the BaY_2ZnO_5 orthorhombic structure when the Dy^{3+} ion concentration is above 20 mol% because BaY_2ZnO_5 and $BaDy_2ZnO_5$ are isostructures with a space group of *Pbnm*. Under ultraviolet (355 nm) excitation, a weak group of emission peaks was observed for the $^4M_{21/2}{}^4I_{13/2} + {}^4K_{17/2} + {}^4F_{7/2} \rightarrow {}^6H_{13/2}$ transition at 453 nm, and two groups of strong emission peaks were observed at 489 nm and 579 nm, corresponding to the $^4F_{9/2} \rightarrow {}^6H_{15/2}$ and $^4F_{9/2} \rightarrow {}^6H_{13/2}$ transitions of Dy^{3+} ions, respectively. The concentration quenching effect occurs for $Ba(Y_{2-x}Dy_x)ZnO_5$ phosphors when x is higher than 0.07, and the critical distance is about 11.93 Å. The CIE color coordinates are $x = 0.320$ and $y = 0.389$, which is in the near-white-light region. The decay curve results show that the decay mechanism of the $^4F_{9/2} \rightarrow {}^6H_{13/2}$ transition is a single decay component between Dy^{3+} ions only. In addition, the asymmetry ratio, which is independent of the Dy^{3+} ion concentration, remains at about 1.04, indicating that the symmetry of Dy^{3+} ions does not change with Dy^{3+} ion concentration.

Acknowledgment

The authors would like to thank the National Science Council of the Republic of China for financially supporting this project under Grant NSC 98-2221-E-150-065-MY2.

References

[1] W.T. Hsu, W.H. Wu, C.H. Lu, Mater. Sci. Eng. B104 (2003) 40.
[2] B.S. Tsai, Y.H. Chang, Y.C. Chen, J. Mater. Res. 19 (5) (2004) 1504.
[3] Y.S. Chang, H.J. Lin, Y.C. Li, Y.L. Chai, Y.Y. Tsai, J. Solid State Chem. 180 (2007) 3076.
[4] R.H. Mauch, Appl. Surf. Sci. 92 (1996) 589.
[5] L. Yi, Y. Hou, H. Zhao, D. He, Z. Xu, Y. Wang, X. Xu, Display 21 (2000) 147.
[6] W.T. Hsu, W.H. Wu, C.H. Lu, Mater. Sci. Eng. B104 (2003) 40.
[7] X. Zhao, X. Wang, B. Chen, Q. Meng, W. Di, G. Ren, Y. Yang, J. Alloy Compd. 433 (2007) 352.
[8] S. Itoh, H. Toki, K. Morimoto, T. Kishino, J. Electrochem. Soc. 138 (1991) 1509.
[9] S. Itoh, M. Yokoyama, K. Morimoto, J. Vac. Sci. Technol. A 5 (1987) 3430.
[10] S. Itoh, T. Kimizuka, T. Tonegawa, J. Electrochem. Soc. 136 (1989) 1819.

[11] C. Feldmann, T. Justel, C.R. Ronda, P.J. Schmidt, Adv. Funct. Mater. 13 (2003) 511.
[12] S.D.H.S.P. Khatkar, V.B.G.S.D.K. Taxak, Mater. Sci. Eng. B 129 (2006) 126.
[13] H. Lai, A. Bao, Y. Yang, W. Xu, Y. Tao, H. Yang, J. Lumin. 128 (2008) 521.
[14] J.A. Kaduk, W. Wing-Ng, W. Greenwood, J. Dillingham, B.H. Toby, J. Res. Natl. Inst. Stand. Technol. 104 (1999) 147.
[15] R.D. Shannon, Acta Crystallogr. A 32 (1976) 751.
[16] K. Hashizume, M. Matsubayashi, M. Vachal, T. Tani, J. Lumin. 98 (2002) 49.
[17] C.H. Liang, X.D. Qi, Y.S. Chang, J. Electrochem. Soc. 157 (5) (2010) 1169.
[18] X.Q. Su, B. Yan, Mater. Chem. Phys. 93 (2005) 554.
[19] Y.C. Li, Y.H. Chang, Y.F. Lin, Y.S. Chang, Y.J. Lin, J. Alloy Compd. 439 (2007) 371.
[20] F.S. Liu, Q.L. Liu, J.K. Liang, J. Luo, L.T. Yang, G.B. Song, Y. Zhang, L.X. Wang, J.N. Yao, G.H. Rao, J. Lumin. 111 (2005) 64.
[21] W.C. Nieuwport, G. Blasse, Soild State Commun. 4 (1966) 227.
[22] Z.J. Kiss, H.A. Weakliem, Phys. Rev. Lett. 15 (1965) 457.
[23] G. Blasse, Philips Res. Rep. 24 (1969) 131.